2024 IEEE/ASME International Conference on Advanced Intelligent Mechatronics (AIM)
July 15-19, 2024. Boston, MA, USA

2024 IEEE/ASME International Conference on Advanced Intelligent Mechatronics (AIM) | 979-8-3503-5536-9/24/$31.00 ©2024 IEEE | DOI: 10.1109/AIM55361.2024.10637226

Cost-Effective Blimp for Autonomous and Continuous Vital Signs Monitoring

Hen-Wei Huang[1,2,3*], Jack Chen[1,3*], Philipp Rupp[1*], Claas Ehmke[2,4*], Peter R Chai[2,5], Riya Dhar[2], Ian Ballinger[1,3] Giovanni Traverso[1,2,3]

***Abstract*—The COVID-19 pandemic renewed interest in contactless vital signs monitoring using computer vision to efficiently screen for disease symptoms. These vital signs monitoring systems have been deployed in either surveillance camera systems or robotic systems. Despite initially promising results, there has been limited uptake. Surveillance cameras are static, which requires subjects to remain inside their field of view during measurement, thus limiting their capacity for continuous monitoring. Robotic systems are mobile and can autonomously track subjects during measurement, but they require expensive software and hardware and tend not to be scalable. In this work, we propose a cost-effective and scalable robotic solution using machine vision microcontrollers to capture photoplethysmography (PPG) information on ambulatory subjects. We characterize the performance of our camera system to design an optimized machine vision protocol to maximize the performance of the machine vision microcontroller for vital signs monitoring. We compared the heart rate estimation accuracy of our cost-effective solution against a state-of-the-art camera (FLIR Blackfly). Our solution achieves a mean average error of 5.0 BPM, comparable to the FLIR Blackfly's mean average error of 4.7 BPM while keeping social distancing (at least 2 meters between cameras and subjects). The major contribution of this work is the design of a machine vision protocol that enables a cost-effective, scalable, and mobile system to achieve the same heart rate estimation accuracy as current state-of-the-art methods.**

I. Introduction

Recent advances in computer vision and artificial intelligence have enabled contactless measurement of vital signs such as heart rate via remote photoplethysmography (rPPG) [1]. These methods have shown great potential during the COVID-19 pandemic by enabling remote assessment of individuals for possible COVID-19 disease [2]. The most straightforward system for rPPG is using surveillance cameras, which require patients to remain static during measurement and remain inside the camera's field of view, preventing continuous monitoring. Motivated by this, we previously proposed a mobile robot system consisting of specialized cameras mounted on Boston Dynamics' quadruped robot Spot. This system was used to facilitate continuous vital signs monitoring for emergency department triage [3]. During its deployment, we learned several factors that limited its translation: ground obstacles in emergency rooms, limited battery capacity of large robots, and costly hardware consisting of the robotic platform, high-spec cameras, and on-board computing units. Together, these factors prevented wide-scale deployment of the robot for use in hospitals. In this work, we propose a cost-effective, aerial, robotic solution to address all of the aforementioned issues.

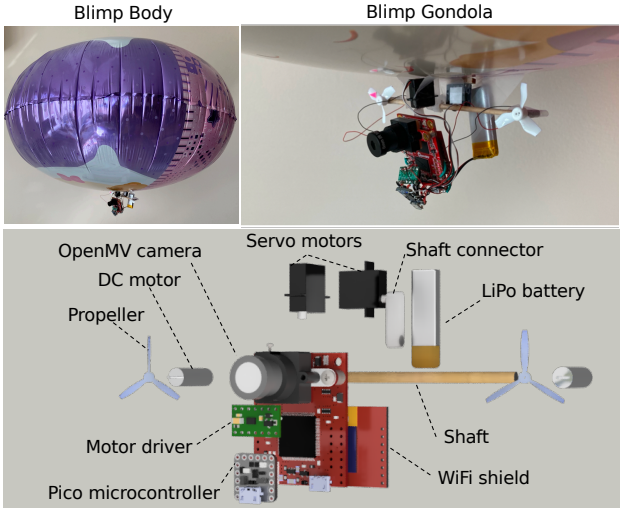

Fig. 1. Robotic blimp for vital signs monitoring consisting of a 32" mylar helium balloon and a gondola. The blimp's machine vision microcontroller coordinates an external PC to perform tasks.

Due to the various ground obstacles in emergency rooms and hospital settings, we desired an aerial robot. We selected miniature blimps as our robotic platform as they are much safer and quieter than drones. As shown in Figure 1, the wireless robotic camera consists of a 36" helium foil balloon with a mounted gondola. An OpenMV H7 Plus (OpenMV) machine vision microcontroller captures rPPG information for heart rate estimation and communicates with an external PC. Unfortunately, this wireless microcontroller can only handle significantly lower image resolution and frame rate compared to its state-of-the-art, wired counterparts. Thus, we designed a novel machine vision protocol that leverages real-time region of interest (ROI) detection and tracking and shares computational loads between the microcontroller and the external PC.

[1]Division of Medicine, Brigham & Women's Hospital, Harvard Medical School, Boston, MA 02115 USA
[2]The Koch Institute for Integrative Cancer Research, Massachusetts Institute of Technology, Cambridge, MA 02142 USA
[3]Department of Mechanical Engineering, Massachusetts Institute of Technology, Cambridge, MA 02139 USA
[4]Multi-Scale Robotics Lab, Department of Mechanical and Process Engineering, ETH Zurich, Tannenstrasse 3, CH-8092, Zurich, Switzerland
[5]Department of Emergency Medicine, Brigham & Women's Hospital, Harvard Medical School, Boston, MA 02115 USA
*Equal Contribution

Authorized licensed use limited to: Nanyang Technological University Library. Downloaded on November 14,2024 at 10:48:26 UTC from IEEE Xplore. Restrictions apply.

The main contributions of this paper are two-fold. First, we describe the development of a cost-effective, easily scalable robotic platform capable of continuous monitoring. Second, we propose a novel wireless machine vision algorithm capable of cutting edge rPPG performance in the cost-effective platform.

II. Related Works

A. Remote Photoplethysmography

Photoplethysmograhy (PPG) is an optical technique that measures changes in light absorption in the capillaries beneath the skin, which corresponds to changes in blood volume. This technique is most commonly used to measure heart rate and blood oxygen saturation, but it can also be used to measure respiration and blood pressure [4]. Remote photoplethysmography (rPPG) refers to contactless methods for PPG. The most common methods use computer vision, but methods have been developed that use radar and wireless technologies [5], which can be leveraged with artifical intelligence for additional applications such as monitoring Parkinson's. In vision-based methods, a camera records a subject and detects or segments a region of interest covering skin pixels. A rPPG algorithm then calculates the pulse signal from the variations in the region of interest. The plane-orthogonal-to-skin (POS) method is one such rPPG algorithm that is motion robust and has previously been demonstrated to correlate with ground truth heart rate estimation [1]. Despite the utility of computer vision methods for rPPG measurement, they restrict movement of the subject and do not enable continuous monitoring. Individuals must enter and remain in the camera's field of view for the entire duration of measurement. In order to improve potential implementation of rPPG for ambulatory subjects, previous work have deployed rPPG on robotic platforms that track and follow subjects [3], [6], [7].

B. Region of Interest

The region of interest (ROI) in an image is the part of an image with relevant information. For instance, the region of interest for object detection is the part of an image containing the object. A common trade-off for cameras is between image resolution and frame rate: increasing one necessarily decreases the other. Our previous work developed a closed-loop ROI algorithm that allows a high-resolution camera to only capture and transmit the relevant region while ignoring redundant information to boost the overall frame rate; furthermore, this works enables a wide field of view to be maintained while tracking fast-moving objects [8], [9].

For rPPG, common ROIs include the forehead, cheeks, and face, which contain large regions of unobstructed skin. Previous work has investigated ROI detection and skin segmentation methods for rPPG [10], [11]. Others have assessed different ROIs and their suitability for rPPG algorithms [12], [13]. Due to the use of facemasks, especially inside hospital settings, the forehead has become more popular and has been confirmed as an excellent ROI for measuring rPPG information with a high signal-to-noise ratio [14], [15].

C. Miniature Robotic Blimps

Miniature robotic blimps are a well-researched robotic platform consisting of a helium balloon with an attached gondola. Small motors and propellers control the blimp's motion, while microcontrollers and sensors enable robotic functionalities. Miniature robotic blimps offer a range of benefits over other aerial robots, including lower cost, lower noise, and increased collision tolerance [16], [17]. Moreover, the robotic blimp does not consume energy to hover, thus resulting in extended battery life. However, blimps are limited by their lower speed, lower durability, and smaller payload [16]. The latter is a particular challenge, as robotic blimps can only carry a very limited set of sensors, batteries, motors, etc. As a result, some work have focused on the optimization of parameters such as number of actuators, [18], gondola placement [19], and communication interface [20].

Previous works have studied and simulated the dynamics of miniature robotic blimps to inform the design of control algorithms [17]. Controlling these blimps is made difficult due to perturbations caused by airflow and buoyancy changes due to leakage and variations in ambient conditions. Some works have designed adaptive motion control algorithms [21], while others have used reinforcement learning to achieve robust control policies capable of withstanding wind disturbance [22], [23]. Functionalities such as localization, navigation, path planning, person following, and teleoperation have all been explored on the robotic blimp platform [24], [25]. Commonly proposed applications for this platform include search and rescue, surveillance, and video broadcasting [26]–[28].

III. Methods

A. Autonomous robotic blimps

The robotic blimp comprises a gondola attached to a mylar foil helium balloon that is 36" in diameter. The gondola is composed of the OpenMV H7 Plus (OpenMV) machine vision microcontroller, the ATWINC1500 WiFi module, a MellBell Pico microcontroller (0.6" x 0.6" package), a Polulu DRV8835 dual DC motor driver, one rechargeable LiPo battery (700 mAh), two mini DC motors with propellers, and two micro servo motors. The two DC motors controlled by the DRV8835 can adjust the speed and direction of the propellers. The two micro servo motors are used to control pitch angle of the propellers and the yaw angle of the OpenMV camera, respectively. The OpenMV is the robot's onboard controller which is in charge of the decentralized computation for capturing high-quality rPPG information; the Pico microcontroller is in charge of blimp locomotion control. The OpenMV and Pico communicate via I2C. The OpenMV communicates via WiFi (ATWINC1500 WiFi module [29]) with an external NVIDIA Jetson AGX Xavier embedded PC (PC). The PC is the centralized computing device that provides high-level control of the robot.

Figure 2 shows the block diagram of robotic camera operations. The blimp begins by rotating in place, transmitting captured images over WiFi to the PC. The PC then detects

Authorized licensed use limited to: Nanyang Technological University Library. Downloaded on November 14,2024 at 10:48:26 UTC from IEEE Xplore. Restrictions apply.

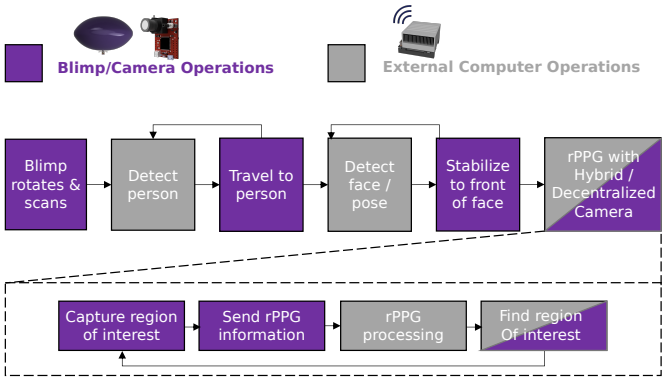

Fig. 2. Block diagram of robotic blimp platform for rPPG. The robot communicates with an external PC to perform operations.

bodies using the YoloV4 object detection model [30]. The blimp travels to a person using the person-detection bounding box as the PID feedback, remaining 2m away at all times. The PC then detects faces using the MTCNN object detection model [31] and Dlib face pose estimation model. Each blimp stabilizes to the person's forehead using the face-detection bounding box and face pose as the PID feedback. The location ROI is critical to the flight control, and a rapidly moving ROI can lead to instability; if the ROI moves out of the field of view, the blimp returns to the rotate and scan phase to relocate the ROI. Finally, the blimp uses the hybrid camera method to stream rPPG video for vital signs estimation.

B. rPPG recording and analyses

To test the proposed camera methods, we applied them to eleven subjects 2m away from the camera. FLIR Blackfly USB3 RGB camera was employed as a reference for benchmarking the performance of the cost-effective wireless camera. Eleven human subjects with various genders, ages, and demography were recruited for evaluating the cost-effective solution. The human subject study was approved by the Institutional Review Board (IRB) of Brigham and Women's Hospital for recording the de-identified facial information. To test parameters that were not camera-specific, we use the UBFC datset, a public rPPG dataset with 43 subject [32].

The POS algorithm is used to analyze the rPPG information to estimate vital signs [1]. Typical rPPG algorithms measures characteristic changes in skin color caused by constriction and dilation and capillaries. The POS algorithm constructs two orthogonal signals from variations in the skin's averaged RGB signal, from which the pulse signal is extracted.

To test the scalability of our solution, we connected five static OpenMV cameras to one external PC wirelessly using the transmission control protocol. All five OpenMV cameras run our proposed rPPG method while simultaneously coordinating with the PC. We measure the frame rate of each camera do determine the effects of multithreading.

C. Wireless machine vision protocols

Figure 3 presents the standard and our proposed machine vision protocol that control the wireless machine vision camera to capture rPPG information. In the standard method, the camera captures and transmits the full-resolution image to an external PC. The PC detects the forehead and computes the RGB average of the pixels covering the forehead. The averaged RGB value are used to analyze the rPPG information via the POS algorithm.

Our proposed method leverages the fact that computing rPPG only requires the forehead, which is a very small region of interest. A small color tracker is placed on the subject's forehead to enable the OpenMV camera to track the forehead. Though this is a rudimentary form of forehead detection, microcontrollers such as the OpenMV do not have the capacity to run more complex models at a reasonable frame rate. For instance, we tested a TensorFlow Lite model for the OpenMV using the COCO Common Objects dataset [33]; unfortunately, this model ran at below 1 FPS on the OpenMV. Color tracking is much simpler and enables real-time, frame-by-frame detection on the OpenMV.

In our proposed method, the PC first takes the full-resolution image to find the location of the subject's face, it then guides the camera to capture the sub-image containing the face. The sub-image, which is the blue bounding box in the Figure 3, allows reasonable head movement while capturing rPPG information without losing color fidelity. In every frame, the OpenMV detects the color tracker and uses its location to estimate the forehead's location. Detection is performed by filtering for color blobs in the narrow range of the color tracker. The OpenMV first calculates the average RGB value of the forehead and only transmits the averaged value to the PC. The PC then directly analyzes the rPPG information. If tracking is lost, the machine protocol resets, and a full-resolution is captured.

Algorithm 1 shows the pseudocode for our proposed machine vision method for rPPG. The machine vision camera initially captures a full resolution image at 2592x1944 pixels. It then uses the color tracker detector to selection a ROI of 1280x720 pixels while also computing the rPPG signal. During vital signs measurement, it is assumed that the subject is stationary. The machine vision camera will automatically capture a new full resolution image every 60 seconds to select the optimal ROI for rPPG.

This method takes advantage of two factors: color detection is a simple algorithm that can run in real time even on embedded processors; rPPG does not actually require images

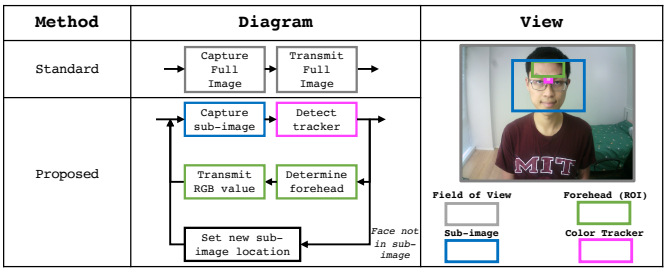

Fig. 3. Overview of the standard and our proposed camera methods for rPPG.

Authorized licensed use limited to: Nanyang Technological University Library. Downloaded on November 14,2024 at 10:48:26 UTC from IEEE Xplore. Restrictions apply.

Algorithm 1 Operations of proposed machine vision protocol for rPPG

```
camera.capture_window = (0, 0, 2592, 1944)
img = camera.capture_image()
tracker = camera.color_detection(img)
ROI_x_loc = (tracker.x - 1280) / 2
ROI_y_loc = (tracker.y - 720 ) / 2
camera.capture_window = (ROI_x_loc, ROI_y_loc, 1280, 720)
timer.start()

while True do
  img = camera.capture_image()
  tracker = camera.color_detection(img)
  forehead = (tracker.x - 250, tracker.y - 100)
  average = camera.compute_RGB_avg(forehead)
  camera.Wifi_transmit_to_PC(average)

  if timer.time() == 60 seconds then
    camera.capture_window = (0, 0, 2592, 1944)
    img = camera.capture_image()
    tracker = camera.color_detection(img)
    ROI_x_loc = (tracker.x - 1280) / 2
    ROI_y_loc = (tracker.y - 720 ) / 2
    camera.capture_window = (ROI_x, ROI_y, 1280, 720)
    timer.restart()

  end if
end while
```

of the skin, and only requires the average RGB values of the skin. Thus, these basic decentralized operations on the OpenMV are sufficient to enable rPPG.

IV. Results and Discussion

Vision-based methods monitor patients from a distance. A camera that is further away from a subject captures subjects at a lower spatial resolution, which results in increased heart rate estimation error as shown in Figure 4. One solution is to reduce the lens' focal length to zoom in on the subject; however, this sacrifices the lens' field of view, reducing subject tracking performance. The other solution is to increase the camera's image resolution; however, this reduces the frame rate, which also results in increased heart rate estimation error as shown in Figure 5. To obtain high accuracy rPPG, it is important to simultaneously have high image resolution at the region of interest and high frame rate. However, the OpenMV camera is limited by its wireless transmission speed: capturing the ROI at maximum image solution results in an overall frame rate of 1 FPS, which is far too low to capture rPPG data.

To address the bottleneck in wireless image transmission, we propose a machine vision protocol that tracks the ROI and only transmit the ROI to an external PC, which computes heart rate from the image data. Since the PC does not receive images covering an entire face, the ROI tracking must be performed by the machine vision microcontroller. In the following subsections, we systematically characterize the performance of our proposed method against the standard method.

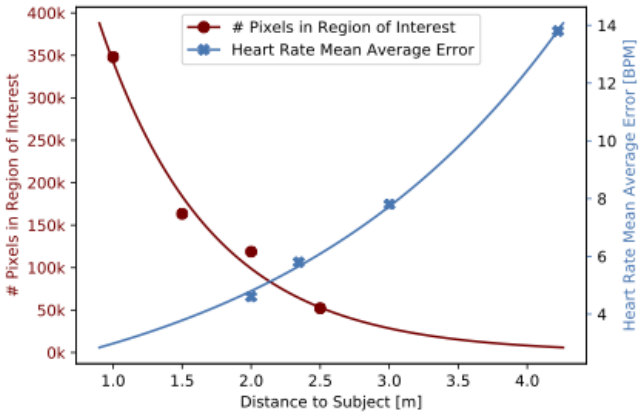

Fig. 4. Frame rate and number of region of interest pixels versus heart rate estimation of rPPG methods.

A. Spatial and temporal resolution characterization

Figure 6 shows the overall comparison of the OpenMV machine vision microcontroller operating at maximum resolution (2592x1944). The standard method operates at 1.0±0.1 FPS, while the proposed method operates at 17.1±0.7 FPS. As expected, the proposed method shows that offloading the ROI detection to the OpenMV and only transmitting image data containing rPPG information greatly boosts the frame rate for all steps.

Here, we will elucidate how each step of the camera and PC operation contributes to the operation speed with varying the processed image resolution. The first step is image capturing. To ensure the forehead is covered by 500 x 200 pixels, the standard method must capture the full field of view at maximum resolution (2592x1944), while the proposed method only needs to capture a smaller region of interest containing the face (1280x720). As shown in Figure 6, this leads to a significant increase in the image capturing speed from 4 FPS to 38 FPS.

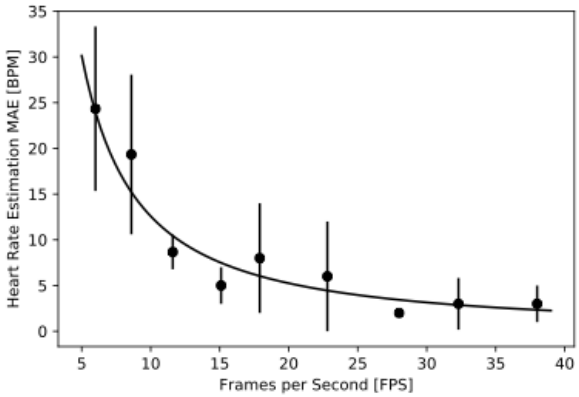

Fig. 5. Frame rate versus heart rate estimation of rPPG methods.

Authorized licensed use limited to: Nanyang Technological University Library. Downloaded on November 14,2024 at 10:48:26 UTC from IEEE Xplore. Restrictions apply.

The second and third steps of the camera methods are image processing and ROI detection. Raw RGB images are too large to be wirelessly transmitted in real-time. JPEG compression significantly reduces image size, but may affect rPPG accuracy as shown in Figure 7. Indeed, greater image compression increases the mean absolute error (MAE), but this effect is limited above a compression factor of 70%. Thus, when using JPEG compression in our camera methods, we use a compression quality factor of 70%.

For the standard method, data processing occurs first under which the image is processed and then wirelessly transmitted to the PC for ROI detection. For the proposed method, ROI detection occurs first under which the color marker is detected, and then the image is processed directly on the machine vision microcontroller. Figure 8 characterizes the data processing step. For the Standard and method, we compress the raw image in JPEG format. For the proposed method, image compression is not required due to the small resolution of the eROI; in fact, performing image compression actually reduces the overall frame rate since due to the time required to perform compression. In the proposed method, the camera computes the raw RGB average of the detected forehead with an image resolution of 500 x 200, requiring 15 ms.

ROI detection is another step that is heavily affected by the image resolution, as shown in Figure 9. For the standard method, the PC detects the forehead ROI from the received image using the MTCNN object detection neural network [31]. The proposed method has significantly higher frame rate because it runs a much simpler color tracker that filters for the specified color range. This strategy allows us to increase the frame rate resolution for ROI while focusing on only the key data necessary to calculate rPPG. Under this circumstance, the proposed achieves 68 FPS for ROI detection, which is faster than the 18 FPS for the standard method.

It is worth noting that the characterization of the ROI detection step may be unfair. Indeed, the proposed method

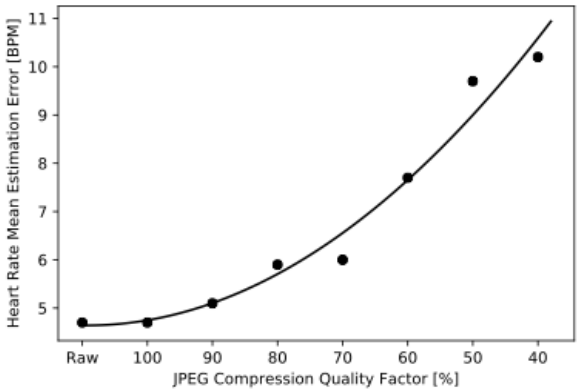

Fig. 7. Effect of JPEG image compression on rPPG accuracy. Raw refers to uncompressed RGB images. Image compression and analysis was performed using the UBFC dataset.

is significantly better, but it only performs color detection while the standard method perform face detection. However, if the standard method used color detection rather than face detection, its frame rate remains at 1.0 FPS. Since ROI detection is not the bottleneck, these insignificant improvements do not lead to higher rPPG accuracy.

The last step that would make difference in frame rate is the wireless data transmission. This is the bottleneck of the standard as it needs to transmit full resolution images. For the standard method, a full-size JPEG image (0.1 MB) must be transmitted, resulting in a frame rate of 2 FPS. For the proposed method, only the RGB average value (1e-5 MB) needs to be transmitted, which can be done instantaneously by the microcontroller's WiFi module. Thus, the porposed achieves 956 FPS for data transmission.

Since we are able to partially offload some computation from the PC to the machine vision camera using the proposed method, a swarm of robotic blimps can be employed to simultaneously monitor multiple subjects using only one central

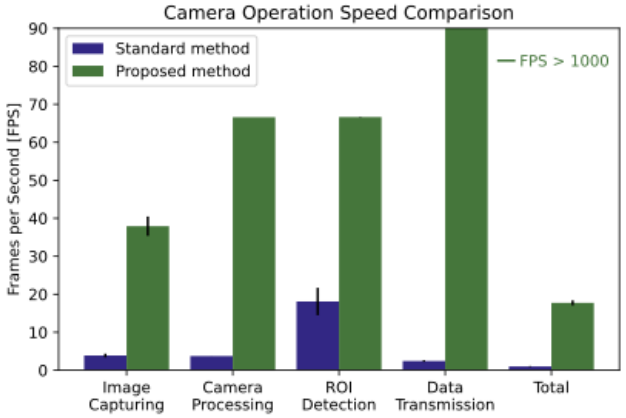

Fig. 6. Operation time and frame rate comparison between camera methods for remote rPPG. Data is collected using the OpenMV machine vision microcontroller at maximum resolution (2592x1944)

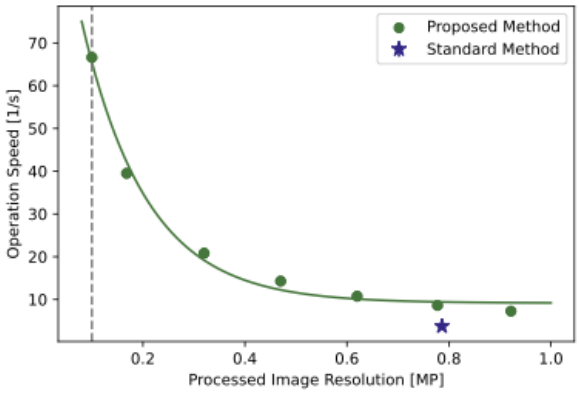

Fig. 8. Characterization of camera processing using the OpenMV machine vision microcontroller. The gray dashed line indicates the exact processed image resolution in the proposed method for image formatting.

Authorized licensed use limited to: Nanyang Technological University Library. Downloaded on November 14,2024 at 10:48:26 UTC from IEEE Xplore. Restrictions apply.

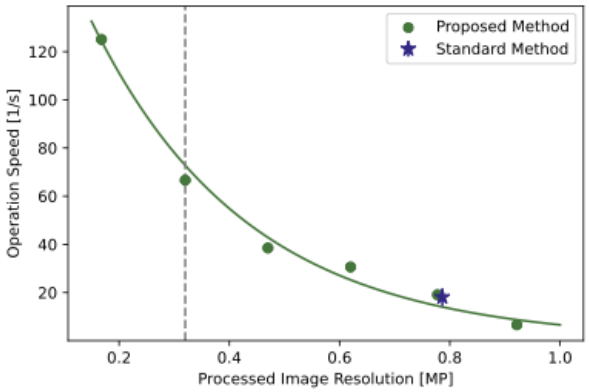

Fig. 9. Characterization of the region of interest detection using the OpenMV machine vision microcontroller (Proposed) and the PC (Standard). The gray dashed line indicates the exact processed image resolution in the proposed method for ROI detection.

PC, thus significantly reducing the overall cost for large-scale deployment. To test the scalability, we established TCP connections between five OpenMV machine vision cameras on the robotic blimps to one central PC via multithreading. During testing, running five OpenMVs in parallel did not cause drops in frame rate for any camera operations.

B. Evaluation of rPPG Estimation Accuracy

To validate the accuracy of the proposed protocols, we employ the USB3 high-resolution FLIR camera capable of capturing rPPG with the same spatial resolution and a significantly high frame rate (40 FPS) as the reference. Figure 10 shows the rPPG accuracy results for nine subjects. The expensive Standard USB3 Camera (FLIR Blackfly with RGB888) achieves accurate performance with a mean average error of 4.7 BPM. The cost-effective, wireless, machine vision camera (OpenMV H7 Plus) with the proposed method–which addresses the bottlenecks in ROI detection and wireless data transmission–achieves comparable performance with a mean average error of 5.0 BPM due to its sufficiently high frame rate (17 FPS) while operating at its maximum spatial resolution (2592x1944). It is shown that the noticeable difference in the frame rate between the FLIR camera and OpenMV with the proposed protocol is not a limiting factor in the rPPG estimation error, a result consistent with Figure 5.

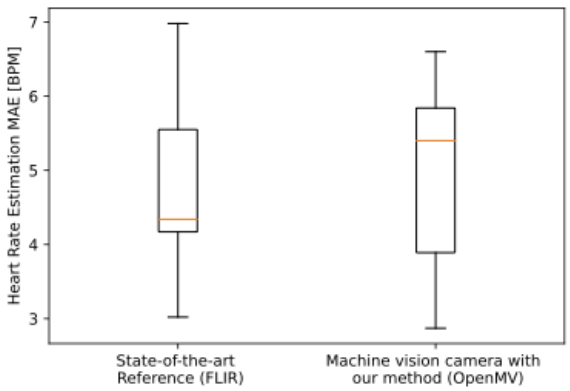

Fig. 10. Accuracy of proposed rPPG methods against standard benchmark for nine subjects. The FLIR Blackfly state-of-the-art camera is used as a benchmark. The proposed methods are deployed on the OpenMV machine vision microcontroller.

V. Conclusion

In this paper, we propose a cost-effective robotic solution with a wireless machine vision microcontroller capable of autonomous, continuous vital sign monitoring. We develop a novel machine vision protocol to enable the cost-effective system to achieve comparable performance to its expensive counterpart. Future work will focus on the deployment and translation of the robot system for patient triage and additional clinical applications.

Acknowledgments

We thank the funding support from Karl Van Tassel (1925) Career Development Professorship, the Department of Mechanical Engineering, MIT, and the Division of Gastroenterology, Brigham and Women's Hospital.

References

[1] W. Wang, A. C. den Brinker, S. Stuijk, and G. de Haan, "Algorithmic principles of remote ppg," *IEEE Transactions on Biomedical Engineering*, vol. 64, no. 7, pp. 1479–1491, 2017.

[2] F. Yang, S. He, S. Sadanand, A. Yusuf, and M. Bolic, "Contactless measurement of vital signs using thermal and rgb cameras: A study of covid 19-related health monitoring," *Sensors*, vol. 22, no. 2, 2022, ISSN: 1424-8220.

[3] H.-W. Huang, J. Chen, P. R. Chai, *et al.*, "Mobile robotic platform for contactless vital sign monitoring," *Cyborg and Bionic Systems*, vol. 2022, 2022.

[4] J. Allen, "Photoplethysmography and its application in clinical physiological measurement," *Physiological Measurement*, vol. 28, R1–39, Apr. 2007.

[5] Y. Rong, P. C. Theofanopoulos, G. C. Trichopoulos, and D. W. Bliss, "A new principle of pulse detection based on terahertz wave plethysmography," *Scientific Reports*, vol. 12, no. 1, 2022.

[6] H. Lee, H. Ko, H. Chung, and J. Lee, "Robot assisted instantaneous heart rate estimator using camera based remote photoplethysmograpy via plane-orthogonal-to-skin and finite state machine," in *2020 42nd Annual International Conference of the IEEE Engineering in Medicine & Biology Society (EMBC)*, 2020, pp. 4425–4428.

[7] H. Lee, H. Ko, H. Chung, and J. Lee, "Real-time realizable mobile imaging photoplethysmography," *Scientific Reports*, vol. 12, 2022.

Authorized licensed use limited to: Nanyang Technological University Library. Downloaded on November 14,2024 at 10:48:26 UTC from IEEE Xplore. Restrictions apply.

[8] J. Chen, H.-W. Huang, P. Rupp, A. Sinha, C. Ehmke, and G. Traverso, "Closed-loop region of interest enabling high spatial and temporal resolutions in object detection and tracking via wireless camera," *IEEE Access*, vol. 9, pp. 87 340–87 350, 2021.

[9] H.-W. Huang, P. Rupp, J. Chen, *et al.*, "Cost-effective solution of remote photoplethysmography capable of real-time, multi-subject monitoring with social distancing," in *IEEE Sensors Conference*, 2022.

[10] P. Li, Y. Benezeth, K. Nakamura, R. Gomez, C. Li, and F. Yang, "Comparison of region of interest segmentation methods for video-based heart rate measurements," in *2018 IEEE 18th International Conference on Bioinformatics and Bioengineering (BIBE)*, 2018, pp. 143–146.

[11] P. Li, Y. Benezeth, K. Nakamura, R. Gomez, and F. Yang, "Model-based region of interest segmentation for remote photoplethysmography," Jan. 2019, pp. 383–388.

[12] D.-Y. Kim, K. Lee, and C.-B. Sohn, "Assessment of roi selection for facial video-based rppg," *Sensors*, vol. 21, no. 23, 2021, ISSN: 1424-8220.

[13] S. Kwon, J. Kim, D. Lee, and K. Park, "Roi analysis for remote photoplethysmography on facial video," in *2015 37th Annual International Conference of the IEEE Engineering in Medicine and Biology Society (EMBC)*, 2015, pp. 4938–4941.

[14] S. Kwon, J. Kim, D. Lee, and K. Park, "Roi analysis for remote photoplethysmography on facial video," English, in *2015 37th Annual International Conference of the IEEE Engineering in Medicine and Biology Society, EMBC 2015*, ser. Proceedings of the Annual International Conference of the IEEE Engineering in Medicine and Biology Society, EMBS, Institute of Electrical and Electronics Engineers Inc., Nov. 2015, pp. 4938–4941.

[15] D.-Y. Kim, K. Lee, and C.-B. Sohn, "Assessment of roi selection for facial video-based rppg," *Sensors*, vol. 21, no. 23, 2021, ISSN: 1424-8220.

[16] J. Hu, A. Bruno, D. Zagieboylo, *et al.*, "To centralize or not to centralize: A tale of swarm coordination," *CoRR*, vol. abs/1805.01786, 2018. arXiv: 1805.01786.

[17] K. Motoyama, H. Kawamura, M. Yamamoto, and A. Ohuchi, "Development of autonomous blimp robot with intelligent control," in *Entertainment Computing: Technologies and Application*, R. Nakatsu and J. Hoshino, Eds. Boston, MA: Springer US, 2003, pp. 191–198.

[18] S. Ferdous, A. Mohammadi, and S. Lakshmanan, "Developing a low-cost autonomous blimp with a reduced number of actuators," in *Unmanned Systems Technology XXI*, May 2019, p. 13.

[19] G. Gorjup and M. Liarokapis, "A low-cost, open-source, robotic airship for education and research," *IEEE Access*, vol. 8, pp. 70 713–70 721, 2020.

[20] R. Al-Jarrah and H. Roth, "Design blimp robot based on embedded system and software architecture with high level communication and fuzzy logic," in *2013 9th International Symposium on Mechatronics and its Applications (ISMA)*, 2013, pp. 1–6.

[21] T. Takaya, H. Kawamura, Y. Minagawa, M. Yamamoto, and A. Ouchi, "Motion control in three dimensional round system of blimp robot," in *2006 SICE-ICASE International Joint Conference*, 2006, pp. 1291–1294.

[22] Y. T. Liu, E. Price, P. Goldschmid, M. J. Black, and A. Ahmad, "Autonomous blimp control using deep reinforcement learning," *CoRR*, vol. abs/2109.10719, 2021. arXiv: 2109.10719. [Online]. Available: https://arxiv.org/abs/2109.10719.

[23] A. Rottmann, C. Plagemann, P. Hilgers, and W. Burgard, "Autonomous blimp control using model-free reinforcement learning in a continuous state and action space," in *2007 IEEE/RSJ International Conference on Intelligent Robots and Systems*, 2007, pp. 1895–1900.

[24] Y. Liu, Z. Pan, D. Stirling, and F. Naghdy, "Q-learning for navigation control of autonomous blimp," Jan. 2009.

[25] N. Yao, E. Anaya, Q. Tao, S. Cho, H. Zheng, and F. Zhang, "Monocular vision-based human following on miniature robotic blimp," in *2017 IEEE International Conference on Robotics and Automation (ICRA)*, 2017, pp. 3244–3249.

[26] Y.-W. Huang, C.-L. Lu, K.-L. Chen, *et al.*, *Duckiefloat: A collision-tolerant resource-constrained blimp for long-term autonomy in subterranean environments*, 2019.

[27] T. Fukao, T. Oshibuchi, K. Osuka, T. Kohno, and Y. Tomoi, "Outdoor blimp robots for rescue surveillance systems," in *2008 SICE Annual Conference*, 2008, pp. 982–987.

[28] T. Fukao, T. Kanzawa, and K. Osuka, "Tracking control of an aerial blimp robot based on image information," in *2007 IEEE International Conference on Control Applications*, 2007, pp. 874–879.

[29] I. Abdelkader, Y. El-Sonbaty, and M. El-Habrouk, *OpenMV: A Python powered, extensible machine vision camera*, 2017. arXiv: 1711.10464.

[30] A. Bochkovskiy, C.-Y. Wang, and H.-Y. M. Liao, *Yolov4: Optimal speed and accuracy of object detection*, 2020. arXiv: 2004.10934.

[31] K. Zhang, Z. Zhang, Z. Li, and Y. Qiao, "Joint face detection and alignment using multitask cascaded convolutional networks," *IEEE Signal Processing Letters*, vol. 23, no. 10, pp. 1499–1503, 2016.

[32] S. Bobbia, R. Macwan, Y. Benezeth, A. Mansouri, and J. Dubois, "Unsupervised skin tissue segmentation for remote photoplethysmography," *Pattern Recogn. Lett.*, vol. 124, no. C, pp. 82–90, Jun. 2019, ISSN: 0167-8655.

[33] T. Lin, M. Maire, S. J. Belongie, *et al.*, "Microsoft COCO: common objects in context," *CoRR*, vol. abs/1405.0312, 2014. arXiv: 1405.0312.

Authorized licensed use limited to: Nanyang Technological University Library. Downloaded on November 14,2024 at 10:48:26 UTC from IEEE Xplore. Restrictions apply.